Premelting features and acoustic mode softening in the rotator phases of linear telomers: $C_{17}H_{36}$

1994 J. Phys.: Condens. Matter 6 10977

(http://iopscience.iop.org/0953-8984/6/50/008)

J. Phys.: Condens. Matter 6 (1994) 10977–10988. Printed in the UK

Premelting features and acoustic mode softening in the rotator phases of linear telomers: $C_{17}H_{36}$

R Jiménez†, J K Krüger†, M Prechtl†, C Grammes† and P Alnot‡
† Fachrichtung Experimentalphysik 10.2, Universität des Saarlandes, Bau 38, Postfach 151150, D-66041 Saarbrücken, Germany
‡ Laboratoire Central de Recherche (LCR), Thompson CSF, F-91404 Orsay Cédex, France

Received 19 May 1994

Abstract. The polymer induced alignment (PIA) technique is presented as a new technique to grow single-crystalline films of linear telomers. Combining the PIA technique with special high-resolution Brillouin techniques, it is possible to determine the coefficients of the elastic stiffness tensor of the crystalline state of linear telomers, especially in their rotator phases. As model systems we have chosen the perfluoroalkane $C_{20}F_{42}$ and the linear n-alkane $C_{17}H_{36}$. A comparison of elastic data obtained from classically and PIA grown samples proves their equivalence as well as their complementarity. Precursors of critical melting discovered in the rotator phase of $C_{17}H_{36}$ are discussed in terms of the anomalous temperature dependence of certain elastic tensor coefficients and of related n-telomers.

1. Introduction

Among other reasons, linear telomers (oligomers), like n-paraffins, perfluoroalkanes, etc, are of great physical interest because of their specific rotator phases (premelting phases), their intricate phase transition behaviour and their model character for related polymers. Special interest has been paid to the physical properties of the crystalline state of n-paraffins and perfluoroalkanes with their specific anisotropic inter- and intramolecular interactions and defects, which are of fundamental interest for the understanding of the phenomenological properties of related macromolecular materials.

The arrangement of covalent bonds within the chain molecules as well as the weak intermolecular interactions strongly affect the mechanical properties, including the elastic anisotropy of telomer crystals consisting of linear chain molecules. In turn, the findings about the static and dynamic elastic properties of these materials contribute to the understanding of the interrelations between their molecular structure, molecular dynamics and morphology, on the one hand, and their outstanding phenomenological properties, on the other. Unfortunately, the determination of the elastic properties of crystalline telomers is found to be much more complicated than it seems to be at first sight [1]. The tendency of this material class to show polymorphism and polytypism makes it difficult to grow sufficiently defectless single crystals [2]. Moreover, the habit and plasticity of solution- and melt-grown samples make it difficult to prepare crystal cuts suitable for ultrasonic and/or Brillouin measurements. Despite all these problems there exists some preliminary work devoted to the description of the elastic behaviour of this substance class. However, until now mainly indirect experimental methods have been discussed in the literature for the determinations of elastic moduli of these materials.

0953-8984/94/5010977+12$19.50

Pechhold *et al* [3] succeeded in measuring the shear stiffness of several n-paraffins in the polycrystalline state as a function of temperature. However, the relation between these shear stiffnesses and those of the single-crystalline state is not evident.

Elastic shear constants of polyethylene microcrystals have been measured by Heyer *et al* [4] using inelastic neutron scattering (INS). This method, developed by Buchenau [5] for application to polycrystalline samples, is based on a statistical treatment of intensity profiles. It has the advantage that no single crystals are needed to determine the elastic properties. However, scattering intensities must be carefully corrected for the spectrometer resolution function and for background scattering. The accuracy obtained with this method is much inferior to that reached by measurements of phonon dispersion curves on single crystals. Furthermore, since INS measures the elastic constants at frequencies in the terahertz range, remarkable differences compared to low-frequency elastic data are to be expected.

A very interesting but still indirect method was used by Strobl [6], who used longitudinal acoustic mode (LAM) frequencies of different orders of $C_{33}H_{68}$ measured by Raman spectroscopy in order to estimate several elastic constants at room temperature.

For the first time Krüger *et al* [7, 8] succeeded by Brillouin spectroscopy in measuring directly several elastic stiffness constants of solution-grown hexatriacontane ($C_{36}H_{74}$) single crystals as a function of temperature. They took advantage of their 90A and 90R scattering geometries [9–11], which allow measurements on crystal plates of only a few micrometres thickness. From their investigations within the rotator phase, an unexpectedly strong decrease of the stiffness modulus c_{33} (propagation of the longitudinal sound mode along the normal to the crystalline layers) with increasing temperature was found. Furthermore, no shear stiffness coefficient c_{44} ($= c_{55}$) was found within this phase, suggesting the possibility that the corresponding shear modes become extremely soft because of a very weak interlayer coupling, indicating the possibility of premelting. Unfortunately, the rotator phases of n-paraffins exist only in narrow temperature intervals, which even decrease with molecular chain length; the premelting process does not really develop in these materials but is passed by true melting. Moreover, the Brillouin measurements on $C_{36}H_{74}$ were performed on crystal plates grown from solution at ambient temperature; the related phase has monoclinic symmetry. In order to reach the solid high-temperature phase (the rotator phase), two strong first-order phase transitions must be passed, which caused ridges and cracks within the sample, obscuring the Brillouin data to a certain extent.

In order to get more insight into the premelting process within the rotator phases indicated by the slowing down of c_{33} of $C_{36}H_{74}$, attention has been focused on fully fluorine-substituted n-alkanes (perfluoroalkanes, C_nF_{2n+2}), which show rotator phases spread over a much wider temperature range than in the case of n-paraffins. As a result, anisotropy inversion of the longitudinal moduli was found in the rotator phase of $C_{16}F_{34}$ and $C_{20}F_{42}$; in addition, an unexpected isostructural premelting transition was found in $C_{20}F_{42}$ by Marx *et al* [12]; a theoretical explanation of this premelting transition was given by Dvorák [13] recently.

In the context of these studies on perfluoroalkanes [12, 14] and semifluorinated alkanes [15], a new efficient Brillouin technique was proposed, which allows, at least in principle, the determination of the complete elastic stiffness tensor from mesoscopic single-crystalline domains of a polydomain film-like sample. For reasons of simplicity we call this technique the thin-film domain (TFD) technique. The main difficulty of the TFD technique is the adjustment of suitable, sufficiently representative, domains for Brillouin measurements [14].

The aim of the current paper is to present a new technique for the preparation of highly oriented crystal mats of linear telomers, which allows the determination of virtually all coefficients of the elastic stiffness tensor of this material class. This so-called polymer

induced alignment (PIA) technique has been proved to be a powerful tool to orient semicrystalline polymers [16–18] as well as liquid crystals [19, 20]. We will show that, at least in the case of linear alkanes and perfluoroalkanes, the PIA technique yields the same rotator phase as found in conventionally grown crystals of the same material. Particularly, in the case of highly symmetric alkane-like crystals, the PIA technique is equivalent to but easier to handle than the TFD technique. For crystals of lower symmetries, the PIA technique is complementary to the TFD technique. As model substances we have chosen $C_{20}F_{42}$ (because we had at our disposal already a great amount of elastic data for comparison) and $C_{17}H_{36}$ (because this n-paraffin is at room temperature in its rotator phase and this phase is sufficiently extended on the temperature scale). The structural properties of both model substances are well known. Those of $C_{17}H_{36}$ were studied by Ungar [21] and Doucet *et al* [22], and those of $C_{20}F_{42}$ were widely studied by Strobl *et al* [23–25]. In the case of $C_{17}H_{36}$, we present and discuss the temperature behaviour of the main stiffness coefficients, focusing our attention on the soft mode behaviour of the longitudinal acoustic mode propagating along the molecular chain axis. We will show that the premelting behaviour already indicated for $C_{36}H_{74}$ [8] and $C_{16}F_{34}$ and definitely found for the perfluoroalkane $C_{20}F_{42}$ [12] and $C_{24}F_{50}$ [26] occurs qualitatively also in the n-paraffin $C_{17}H_{36}$, indicating the existence of a rather universal premelting tendency in the rotator phase of alkane-like materials.

2. Experimental details

2.1. Sample preparation

The TFD sample preparation technique has been discussed recently in detail by Marx *et al* [14] and therefore needs only a few comments. As a sample holder we used a sandwich consisting of two glass slides and polyimide spacers of about 15 μm thickness. The molten sample was introduced into the cell using the capillarity effect. Afterwards the sample was cooled down slowly to the rotator phase in order to form as large monodomains as possible. Monodomains with lateral dimensions of 50–100 μm could be produced.

The PIA technique uses the fact that linear polymer and oligomer molecules tend to align themselves with their molecular chain axes on crystalline polytetrafluoroethylene (PTFE) along the unique axis of the PTFE. The method is based on the deposition of a highly oriented and highly crystalline PTFE layer of about 10 nm thickness on a smooth glass surface. The deposition of the layer takes place by rubbing a PTFE rod on a clean glass slide at elevated temperatures, thus mechanically inducing a perfect orientation of the PTFE crystallites with their unique axes pointing along the rubbing direction. Because of their efficient alignment influence on linear polymers [16–18] and related materials, for example liquid crystals [19, 20], we denote such a supporting PTFE film as a PIA substrate.

The growth of thin crystalline n-telomer film (for instance of $C_{17}H_{36}$) on the PIA substrate occurs in such a way that the molecules of the deposited substance show an outstanding unidirectional texture and that the textured thin film consists of a highly textured crystal mat having the crystallographic c axis of the quasi-hexagonal lattice of the rotator phase [21, 22] aligned along the rubbing direction of the PTFE substrate and possibly one further crystallographic axis within the substrate plane (see below). To date there are only preliminary ideas about the precise transcrystallization mechanisms induced by the PIA substrate [16].

It is evident that the PIA effect decreases with increasing sample thickness; for a given thickness of a film-like sample the PIA effect can be enhanced, by increasing the effective surface, using a PIA coated glass sandwich as sample holder, schematically shown in figure 1.

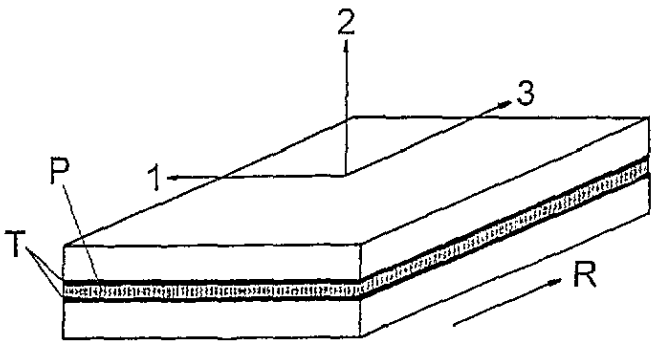

Figure 1. Schematic representation of a PIA coated glass sandwich used to prepare the telomer samples for Brillouin spectroscopic experiments. R, rubbing direction of the PTFE rod; T, PTFE layer; P, sample. The coordinate system has been chosen to keep the 3 axis parallel to the PTFE rubbing direction.

The filling procedure of the sandwich cell is the same as in the case of the TFD technique. Sample thicknesses range typically between 1 and 5 μm.

The model samples investigated in this work were purchased from Merck ($C_{17}H_{36}$) and Hoechst ($C_{20}F_{42}$) and have the usual commercial purity grade. $C_{20}F_{42}$ has its melting temperature at $T_m = 434$ K and shows structural phase transitions at 198 and 147 K [12]. At ambient temperature $C_{20}F_{42}$ has a trigonal rotator phase, which, in this special case, is nearly hexagonal (quasi-hexagonal); from the elastic point of view the material behaves as completely hexagonal [12]. $C_{17}H_{36}$ has its melting temperature at $T_m \simeq 295$ K and a further structural transition at $T_c \simeq 283$ K [22]. Between T_c and T_m, $C_{17}H_{36}$ has an orthorhombic rotator phase, which becomes increasingly hexagonally structured on approaching T_m [21, 22].

2.2. Brillouin spectroscopy

Taking advantage of the 90A scattering geometry [9, 27, 28], one can obtain information about the elastic constants in thin films by means of Brillouin spectroscopy (BS). Moreover, the use of angular and space resolving BS [18, 29] allows the determination of almost all the elastic constants present in the elastic stiffness tensor of the crystalline state using exclusively polydomain film-like samples. The corresponding phonon wavevector q is contained within the PIA film plane, and the relation between sound velocity v^{90A} and phonon frequency f^{90A} is

$$v^{90A} = f^{90A}\lambda_0/\sqrt{2} \tag{1}$$

where λ_0 is the laser wavelength in vacuum (514.5 nm in our case). As has been discussed elsewhere [11], the acoustic wavelength depends little, or in many cases not at all, on the optical refraction properties of the sample. The stiffness coefficient c, related to the measured sound frequency, obeys the relation $c = \rho v^2$ where ρ is the mass density of the material. Measuring the phonon frequency for different directions of the q vector within the film plane and taking into account the relevant symmetry of the sample under study, one can solve the Christoffel equation (e.g. [30]), yielding the desired stiffness coefficients c_{kl}. The basic relation for the determination of the elastic stiffness tensor **c** written in matrix notation is given by

$$\det[\mathbf{lcl}^{\mathrm{T}} - \mathbf{E}c'(p, q)] = 0 \tag{2}$$

with

$$l = \begin{pmatrix} l_1 & 0 & 0 & 0 & l_3 & l_2 \\ 0 & l_2 & 0 & l_3 & 0 & l_1 \\ 0 & 0 & l_3 & l_2 & l_1 & 0 \end{pmatrix} \tag{3}$$

and $\mathbf{c} = \{c_{kl}\}$ is the fourth-rank elastic tensor in shortened 6×6 Voigt notation. It is in general a complex tensor and these equations hold strictly only if the condition $c' \gg c''$ between real part (c') and imaginary part (c'') is fulfilled. $\boldsymbol{E}$ is a 6×6 unity matrix. The l_i ($i = 1, 2, 3$) are direction cosines, which define the direction of the wavevector $\hat{q} = (l_1, l_2, l_3)$. The right-handed orthogonal coordinate directions {1, 2, 3} have been chosen according to figure 1. For hexagonal symmetry the elastic stiffness tensor has the following form (Voigt notation):

$$\begin{bmatrix} c_{11} & c_{12} & c_{13} & & & \\ c_{12} & c_{11} & c_{13} & & 0 & \\ c_{13} & c_{13} & c_{33} & & & \\ & & & c_{44} & & \\ & 0 & & & c_{44} & \\ & & & & & c_{66} \end{bmatrix} \tag{4}$$

with $c_{66} = (c_{11} - c_{12})/2$. The 3 axis points along the rubbing direction of the PIA film and the 2 axis is directed orthogonal to the PIA sandwich. For the (1,3) plane $\hat{q} = (\sin\theta, 0, \cos\theta)$ holds (see polar plots).

Using a cryostat allowing angle-dependent Brillouin spectroscopy, we were able to determine the elastic stiffness components of $C_{17}H_{36}$ as a function of temperature.

The determination of the refractive index ellipsoid has been performed with an Abbé refractometer (Zeiss, model A) and a polarization microscope (Leitz, Laborlux) with a Berek tilting compensator (Leitz) and a universal rotating table (Leitz).

3. Results and discussion

In order to study the efficiency of the PIA technique as a convenient crystal growth method for linear telomers, we prepared a thin film of $C_{20}F_{42}$ in a PIA sandwich (see section 2). Subsequently we performed angular-dependent Brillouin investigations of the rotator phase at room temperature using the 90A scattering geometry and compared the obtained data with those measured by Marx *et al* [12], who used the TFD technique. Figure 2 shows the related sound velocity polar plots. Because of the small thickness d of our PIA sample ($d \leqslant 5\ \mu$m), the scattering cross section for the transverse and quasi-transverse phonon was so small that the appropriate phonon branch could not be detected. Taking into account that methodical errors like the adjustment of the inner and outer scattering angles, temperature, etc, may easily produce an absolute error of some per cent in the sound velocity, the observed agreement between both data sets seems to be very good and confirms the equivalence of the PIA and TFD techniques. The related elastic stiffness coefficients estimated from the sound velocity data and the density $\rho(298\ \text{K}) = 2147\ \text{kg m}^{-3}$ taken from Marx *et al* [12] are given in table 1.

Figure 2 verifies the assumption made before related to the orientation of the crystalline c axis in the film plane on the PIA substrate. It turns out that, as in the case of polymers and liquid crystals, the molecular chain axes point along the rubbing direction of the PTFE substrate.

Table 1. Elastic stiffness coefficients of $C_{20}F_{42}$ at $T = 298 \pm 1$ K.

	This work	Marx *et al* [12]
c_{11} (GPa)	6.2 ± 0.4	5.8 ± 0.3
c_{33} (GPa)	$8.5 \bullet 0.4$	8.0 ± 0.3
c_{13} (GPa)	—	1.1 ± 0.2
c_{44} (GPa)	—	0.03 ± 0.03
ρ (kg m^{-3})	2147	2147

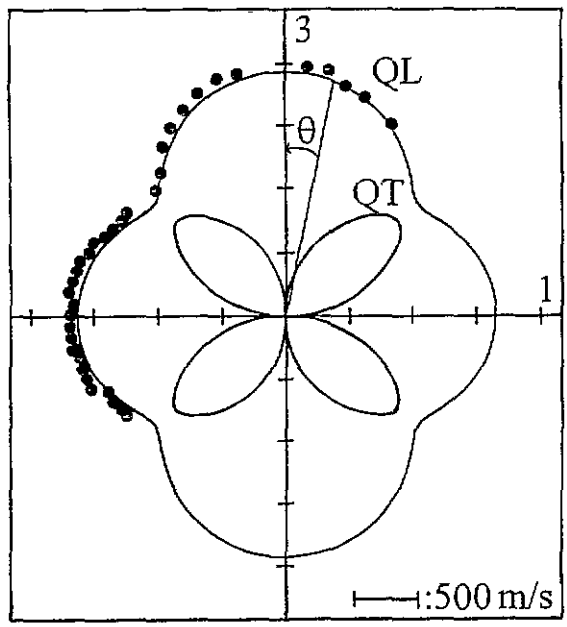

Figure 2. Sound velocity polar plot of $C_{20}F_{42}$ in the 1,3 plane ($T = 298$ K). Full circles represent the experimental data. The full curve represents the results of [12]. QL, quasi-longitudinal branch; QT, quasi-transverse branch; θ, angle between q and 3 axis.

As a second model substance with an inherent rotator phase we have chosen the linear n-alkane $C_{17}H_{36}$. In order to get as much information as possible about the elastic properties, we performed PIA as well as TFD measurements. In a first step we investigated the temperature dependence of the sound velocity of a quasi-longitudinal (QL) polarized phonon at a polar angle $\theta \simeq 45°$ (figure 3) in order to control whether the PIA-prepared $C_{17}H_{36}$ film had the same structure and, as a consequence, the same phase transition temperature as the raw material. Below $T_c \simeq 283$ K a clear splitting of the quasi-longitudinal polarized phonon branch is observed, indicating a further lowering of the crystal symmetry. The observed transition temperature is in perfect agreement with that given in section 2 for the raw crystalline material, indicating thus that we prepared the desired rotator phase on the PIA substrate.

For technical reasons the angular-resolving Brillouin measurements on PIA- and TFD-prepared samples were performed at $T = 287$ K and 291 K respectively. At these temperatures the samples are expected to have orthorhombic symmetry [21, 22]. Figures 4 and 5 show the corresponding sound velocity polar plots. In contrast to our results on $C_{20}F_{42}$, we were able to detect the quasi-transverse (QT) branches.

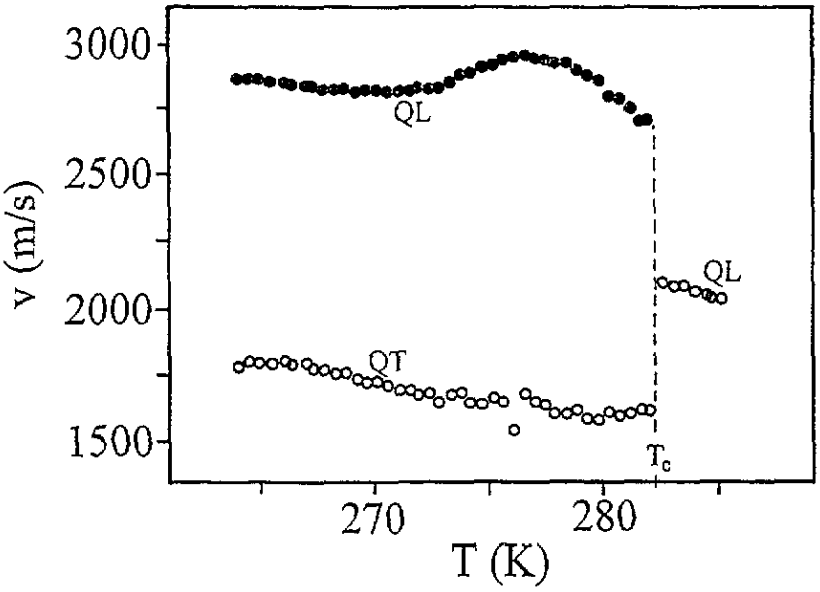

Figure 3. Temperature dependence of the quasi-longitudinal phonon (QL) in the rotator phase ($T > T_c$) and in the low-temperature phase ($T < T_c$) of $C_{17}H_{36}$. QT, quasi-transverse phonon.

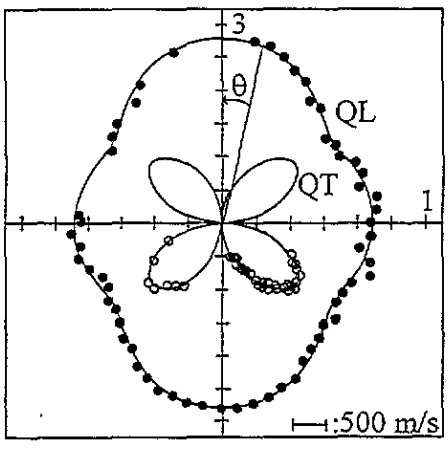

Figure 4. Sound velocity polar plot in the 1, 3 plane (T = 287 K) of $C_{17}F_{36}$ on PIA substrate. Open and full circles represent the experimental data. Full curves represent the results for the quasi-longitudinal branch (QL) and quasi-transverse branch (QT) from the least-squares fit of equation (2) to the experimental data. θ, angle between q and 3 axis.

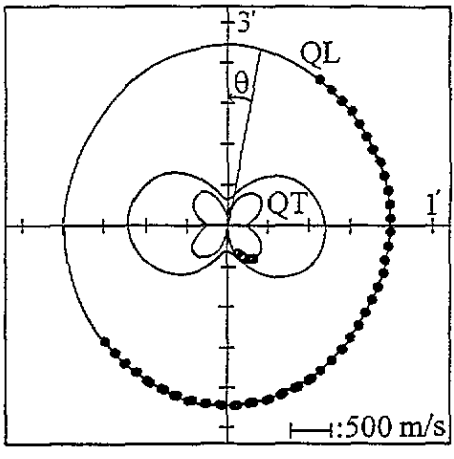

Figure 5. Sound velocity polar plot in the 1, 3 plane (T = 291 K) of a TFD-prepared $C_{17}F_{36}$ sample. Open and full circles represent the experimental data. Full curves represent the results for the quasi-longitudinal branch (QL) and quasi-transverse branch (QT) from the least-squares fit of equation (2) to the experimental data (for more explanation, see text). In this case the orientation of the domain is random with respect to the glass sandwich coordinate system, and therefore we use 3' and 1' instead of 1 and 3. θ, angle between q and 3' axis.

As a consequence of the preparation technique, the orientation of the domain used for the TFD measurement is expected to be random with respect to the laboratory coordinate system. In case of the PIA sample, at least the crystallographic c axis is oriented in the film plane. From figure 4 it follows that the sound velocity has its maximum along the rubbing direction of the PTFE substrate, which, indeed, confirms that the c axis of the rotator phase of $C_{17}H_{36}$ has the same orientation as the preferential direction of the PTFE molecules. Additional measurements of the optical refraction behaviour with an Abbé refractometer yield three different refractive indices $n_1 = 1.441$, $n_2 = 1.477$ and $n_3 = 1.525$, thus confirming the presence of the expected orthorhombic symmetry at $T = 293$ K. From these measurements and additional birefringence measurements of several different domains of the TFD sample with a polarization microscope using tilting compensators and a universal rotating table, we conclude that the 1 axis and the 2 axis of the PIA sample correspond to the main axes of the index ellipsoid and, as a consequence, they correspond to the crystallographic axes of the orthorhombic rotator phase. This result is in agreement with observations on vinylidene polymers and oligomers, where also the c axis and one further crystallographic axis were found to be directed within the film plane of the PIA-prepared samples [31].

Table 2. Elastic stiffness coefficients of $C_{17}H_{36}$ grown on PIA substrate at $T = 287$ K as calculated from the data of figure 4.

c_{11} (GPa)	4.43 ± 0.05
c_{22} (GPa)	4.4 ± 0.1
c_{33} (GPa)	6.96 ± 0.07
c_{13} (GPa)	2.52 ± 0.08
c_{44} (GPa)	$\gtrsim 0$
ρ (kg m^{-3})	890.7

The data of figure 4 have been used to determine the stiffness coefficients c_{11}, c_{33} and c_{13} performing a least-squares fit with equation (2) to the measured data (table 2). The density values necessary for calculation of the stiffness coefficients were calculated from the lattice parameters given by Ungar [21]. For reasons of elastic stability the shear stiffness c_{44} has to be larger than zero but appeared to be so close to zero that, within the margin of error, we could not fit a reliable value larger than zero to the data. In order to determine the stiffness coefficient c_{22} we performed Brillouin measurements using the 90R scattering geometry [11] with the electric field vectors of the incident and scattered light directed along the 1 axis of the PIA sample. The relations between the measured sound frequency, the sound velocity and the desired stiffness coefficient are as follow:

$$v^{90R}(\hat{q}\|2) = f^{90R}(\hat{q}\|2)\lambda_0/(4n_1^2 - 2)^{1/2} \tag{5}$$

$$c_{22} = \rho(v^{90R})^2. \tag{6}$$

As a matter of fact we found $c_{22} \simeq c_{11}$ (table 2); this means that, from the elastic point of view, $C_{17}H_{36}$ behaves as quasi-hexagonal at the temperature in question even though the crystal structure is clearly not [21].

We have extended the 90A and 90R measurements to the entire rotator phase of the PIA sample. Figure 6 shows the complete results. Taking the values for c_{11}, c_{22}, c_{33}, c_{13} and c_{44} from figure 6 at $T = 291$ K as fixed parameters and fitting the sound velocity data obtained from 90A measurements of the TFD sample (figure 5) using Christoffel's equation (2), we obtained the complete elastic stiffness tensor for this temperature (table 3).

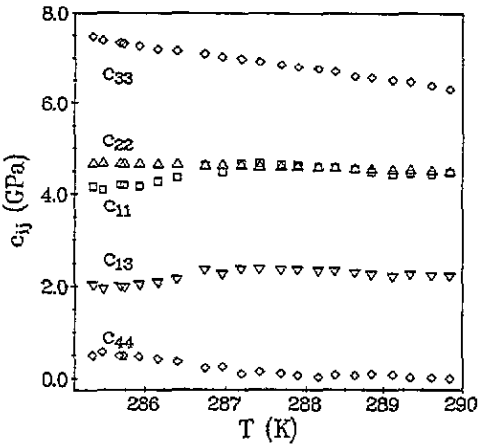

Figure 6. Temperature dependence of the elastic constants c_{ij} of the rotator phase of $C_{17}F_{36}$.

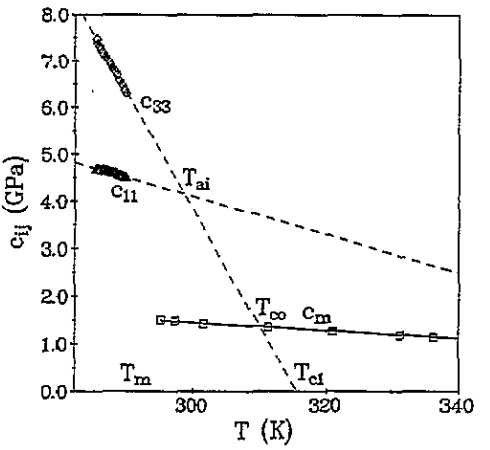

Figure 7. Temperature dependence of the elastic stiffness coefficients c_{11}, c_{33} and c_m (elastic constant in the melt). The broken lines represent the extrapolation of the c_{11} and c_{33} values to higher temperatures. The full line shows the temperature dependence of c_m. T_m is the melt transition temperature. T_{ai}, T_{co}, T_{cl} are explained in the text.

Table 3. Elastic stiffness coefficients of $C_{17}H_{36}$ at $T = 291$ K obtained from Brillouin measurements made on PIA and TFD samples.

c_{11} (GPa)	4.43*
c_{22} (GPa)	4.47*
c_{33} (GPa)	6.20*
c_{13} (GPa)	2.21*
c_{44} (GPa)	$\gtrsim 0$*
c_{55} (GPa)	$\gtrsim 0$*
c_{66} (GPa)	0.32 ± 0.006
c_{12} (GPa)	4.26 ± 0.01
c_{23} (GPa)	1.70 ± 0.05
ρ (kg m^{-3})	885

* Denotes values that were obtained purely from a PIA sample and fixed during the least-squares fitting procedure (for further explanations, see text).

Concerning $c_{33}(T)$, the temperature dependence of this elastic constant reveals a similar behaviour to that found for the rotator phases of $C_{36}H_{74}$ [8] and of the perfluoroalkanes $C_{16}F_{34}$ and $C_{20}F_{42}$ [12]. In accordance with the orthorhombic symmetry of the rotator phase of $C_{17}H_{36}$, we find at lower temperatures a significant splitting of c_{11} and c_{22}, which disappears at about 287 K. Above this temperature both quantities coincide up to the melt transition, reflecting from the elastic point of view a hexagonal behaviour. According to Ungar [21] the hexagonal character of the rotator phase becomes increasingly pronounced approaching the melting temperature but $T = 287$ K has no special meaning within the reported lattice parameter curves. The magnitude used to describe the hexagonal character of the crystal lattice is the a/b ratio, where a and b are the lateral dimensions of the unit cell: $a/b = \sqrt{3}$ is the characteristic value for a hexagonal subcell. In the case of $C_{17}H_{36}$ the a/b ratio increases steeply with increasing temperature; at $T = 287$ K a/b is about

1.513 and increases up to 1.55 at T_m, which is, in contrast to the elastic degeneracy of c_{11} and c_{22}, still far away from $\sqrt{3}$.

The most striking feature of the elastic properties shown in figure 7 is the strong decrease of c_{33} with increasing temperature and the anisotropy inversion (a) above $T_{ai} = 298$ K, yielding $a = (c_{33}/c_{11}) \leqslant 1$. This anisotropy inversion implies that the series connection of the van der Waals and the covalent interaction forces, responsible for the stiffness c_{33}, becomes significantly smaller than the pure van der Waals interaction forces, responsible for the stiffnesses c_{11} and c_{22}, although the intramolecular covalent C–C bonds are strong compared to the lateral intermolecular van der Waals bonds between the molecular chains.

Table 4. Elastic stiffness temperature gradients and Grüneisen parameters of various linear telomers for their rotator phase. T_{c1} is the premelting temperature of the lamellae stacking [12].

				$C_{20}F_{42}$	
	$C_{17}H_{36}$	$C_{36}H_{74}$	$C_{16}F_{34}$	$T < T_{c1}$	$T > T_{c1}$
dc_{33}/dT (GPa K^{-1})	-0.25 ± 0.03	-5 ± 1	-0.06 ± 0.01	-0.07 ± 0.01	-0.01 ± 0.02
dc_{11}/dT (GPa K^{-1})	-0.04 ± 0.01	-0.1 ± 0.1	-0.02 ± 0.01	-0.02 ± 0.01	-0.02 ± 0.01
γ_3	14.8	—	—	—	—
γ_1	2.9	—	—	—	—

The temperature gradient dc_{33}/dT is about six times larger than $dc_{11}/dT \simeq dc_{22}/dT$ (see table 4). It turns out that dc_{11}/dT is of the same order for all investigated n-telomers. The value of dc_{33}/dT always strongly exceeds the value of dc_{11}/dT (table 4) and a large difference appears between n-alkanes and perfluoroalkanes. Moreover, a significant increase is observed for increasing molecular chain lengths of the same species.

No hypersonic attenuation anomalies have been observed for the investigated phonon branches within the rotator phase of $C_{17}H_{36}$. Particularly, the longitudinal acoustic phonon propagating along the 3 axis shows no anomalous attenuation behaviour as a function of temperature, indicating thus that the strong softening of this mode is a purely static property. Therefore, as in the case of $C_{20}F_{42}$, we can tentatively describe the longitudinal modulus c_{33} by a Curie–Weiss law [32], $\Delta c_{33} = (c_{33} - c_{33}^0) \propto A|T - T_{c1}|$, where c_{33}^0 is the uncritical part of the modulus c_{33}, A is the Curie–Weiss constant and T_{c1} (= 315 K) is the hypothetical transition temperature. The Curie–Weiss behaviour suggests a linear coupling between the hypothetical order parameter and the elastic strain component ε_3 (Voigt notation). Following the ideas of Marx *et al* [12], T_{c1} would correspond to an interlamellar melting temperature. However, as shown in figure 7, the extrapolated $c_{33}(T)$ curve intersects the curve of the melt modulus $c_m(T)$ at $T_{c0} = 308$ K, which is well below T_{c1}. In spite of the fact that the shear stiffness $c_{44} \simeq c_{55}$ is already close to zero, suggesting a very weak coupling between adjacent layers, both stability limits (T_{c0} and T_{c1}) are overtaken by intralamellar melting. In context with the anomalous decrease (softening) of $c_{33}(T)$ within the rotator phase, it should be mentioned that the lattice parameter c remains nearly constant within this phase [21, 22], thus indicating changes of the elastic interactions due to structural rearrangements in between the crystal lamellae, which hardly affect the lattice parameters. The importance of the interlayer regions for the elastic stiffness c_{33} is also supported by the fact that the longitudinal acoustic mode (LAM) frequency measured by Raman spectroscopy generally yields a nearly temperature-independent stiffness modulus of the single lamella c_{33}^{LAM} of more than 100 GPa [6, 12]; thus, the elastic series connection of c_{33}^{LAM} and the interlayer modulus is dominated by the latter. In order to support this view we have combined the

main longitudinal phonon frequencies $\omega_{L1} = 2\pi f_{L1}$ (phonon propagation along the 1 axis) and $\omega_{L3} = 2\pi f_{L3}$ (phonon propagation along the 3 axis), both measured as a function of temperature, with the volume of the unit cell v_c calculated from the lattice parameters given by Ungar [21]. Taking the temperature as a parameter, we calculated the almost linear curves given in figure 8. It is evident that ω_{L3} changes much more drastically as a function of v_c than does ω_{L1}. Defining

$$\gamma_{Li} = \partial \ln \omega_{Li} / \partial \ln v_c \qquad i = 1, 2, 3 \tag{7}$$

as longitudinal-mode Grüneisen parameters for phonon propagation along the i axis, we obtain from figure 8 that γ_{L3} has an anomalously high value of 14.8 whereas $\gamma_{L1} = 2.9$ behaves quite normally (see table 4). The apparent large anharmonicity reflected by γ_{L3} is believed to be a consequence of an increasing longitudinal translational disorder of the chain molecules [12].

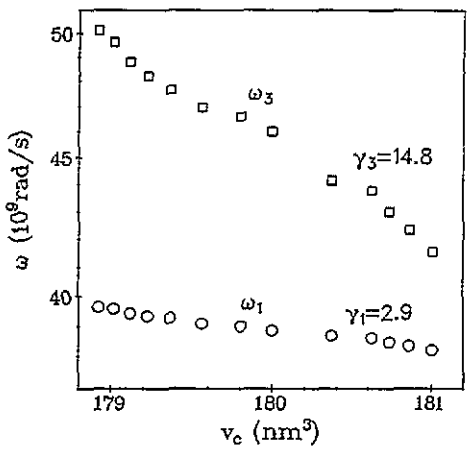

Figure 8. Dependence of the phonon frequencies ω_1 and ω_3 on the unit-cell volume v_c. γ_i ($i = 1, 3$) represents the calculated mode Grüneisen parameters. Notice that both axes show logarithmic scales.

A more recent theoretical approach presents an explanation for the temperature behaviour of c_{33} in the case of the rotator phase of $C_{20}F_{42}$ in the frame of Landau's theory [13]. In this work the order parameter η is related to the ABC stacking of the lamellae within the crystal. Moreover, this order parameter couples quadratically to the elastic deformation ε_3 (relevant coupling term $\eta^2\varepsilon_3$) and produces a change of slope in $c_{33}(T)$ at a definite temperature T_c, which can be considered as an interlamellar melting point, giving rise to a statistically distributed hexagonal packing of A, B and C lamellae. However, it is not yet clear whether this model can be translated to the case of $C_{17}H_{36}$. Anyway, only a precursor of this transition is seen in the case of $C_{17}H_{36}$: the transition itself is shadowed by the real first-order melting transition. Especially, the predicted jump of c_{33} at the transition cannot be verified because the related transition temperature is already in the molten state.

4. Conclusions

Within this paper we have presented a new crystal growth technology (PIA technique) that allows quick preparation of single-crystalline films of n-telomers having at least one

well defined crystal axis with respect to the coordinate system of the growth substrate. Such crystal films are especially suitable for 90A Brillouin investigations of their elastic tensor properties. As model substances we investigated $C_{17}H_{36}$ and $C_{20}F_{42}$. Comparative measurements on $C_{20}F_{42}$ with the PIA and TFD techniques have proven the equivalence and/or complementarity of both methods. This complementarity has been used in order to determine the complete elastic tensor of $C_{17}H_{36}$ at $T = 291$ K. For the rotator phase of this material we were able to determine the most important elastic stiffness coefficients as a function of temperature using high-performance Brillouin spectroscopy. The softening of the longitudinal polarized acoustic mode represented by c_{33} is discussed in terms of a successive interlayer melting process. The stiffness modulus $c_{33}(T)$ seems to follow a Curie–Weiss law. It turns out that n-alkanes and perfluoroalkanes behave similarly concerning their premelting tendency. Further experimental and theoretical work is in progress.

References

[1] Krüger J K 1989 *Optical Techniques to Characterize Polymer Systems* ed H Bässler (Amsterdam: Elsevier)
[2] Boistelle R 1980 *Current Topics in Material Science* vol 4, ed E Kaldis (Amsterdam: North-Holland)
[3] Pechhold W, Dollhopf W and Engel A 1966 *Acustica* **17** 61
[4] Heyer D, Buchenau U and Stamm M 1984 *J. Polym. Sci.* **22** 1515
[5] Buchenau U 1979 *Solid State Commun.* **32** 1329
[6] Strobl G R and Eckel R 1976 *J. Polym. Sci.* **14** 913
[7] Krüger J K, Bastian H, Asbach G I and Pietralla M 1980 *Polym. Bull.* **3** 633
[8] Krüger J K, Pietralla M and Unruh H-G 1982 *Phys. Status Solidi* a **71** 493
[9] Krüger J K, Peetz L and Pietralla M 1978 *Polymer* **19** 1397
[10] Krüger J K, Pietralla M and Unruh H-G 1983 *Colloid. Polym. Sci.* **261** 409
[11] Krüger J K, Marx A, Peetz L, Roberts R and Unruh H-G 1986 *Colloid. Polym. Sci.* **264** 403
[12] Marx A, Krüger J K and Unruh H-G 1989 *Z. Phys.* B **75** 101
[13] Dvorák V and Holakovský J 1993 *Ferroelectrics* **145** 23
[14] Marx A, Krüger J K and Unruh H-G 1988 *Appl. Phys.* A **47** 367
[15] Marx A, Krüger J K, Kirfel A and Unruh H-G 1990 *Phys. Rev.* B **42** 6642
[16] Wittmann J C and Smith P 1991 *Nature* **352** 414
[17] Krüger J K, Prechtl M, Smith P, Meyer S and Wittmann J C 1992 *J. Polym. Sci.* B **30** 1173
[18] Krüger J K, Prechtl M, Wittmann J C, Meyer S, Legrand J F and D'asseza G 1993 *J. Polym. Sci.* B **31** 505
[19] Grammes C, Krüger J K, Bohn K-P, Baller J, Fischer C, Schorr C, Rogez D and Alnot P 1994 *Phys. Rev.* E at press
[20] Krüger J K, Grammes C, Jiménez R, Schreiber J, Bohn K-P, Baller J, Fischer C, Rogez D, Schorr C and Alnot P 1994 *Phys. Rev.* E at press
[21] Ungar G 1983 *J. Phys. Chem.* **87** 689
[22] Doucet J, Denicolo I and Craievich A 1981 *J. Chem. Phys.* **75** 1523
[23] Schwickert H, Strobl G and Kimmig M 1991 *J. Chem. Phys.* **95** 2800
[24] Albrecht T, Elben H, Jaeger R, Kimmig M, Steiner R, Strobl G, Stühn B, Schwickert H and Ritter C 1991 *J. Chem. Phys.* **95** 2807
[25] Albrecht T, Jaeger R, Petry W, Steiner R, Strobl G and Stühn B 1991 *J. Chem. Phys.* **95** 2817
[26] Jiménez R, Krüger J K, Fischer C, Bohn K-P, Dvorák V, Holakovský J and Alnot P 1994 *Phys. Rev.* B at press
[27] Krüger J K, Sailer E, Spiegel R and Unruh H-G 1978 *Prog. Colloid Polym. Sci.* **64** 208
[28] Krüger J K, Peetz L, Siems R, Unruh H-G, Eich M, Herrmann-Schönherr O and Wendorff J H 1988 *Phys. Rev.* A **37** 2637
[29] Krüger J K, Jiménez R, Bohn K-P, Petersson J, Albers J, Klöpperpieper A, Sauerland E and Müser H-E 1990 *Phys. Rev.* B **42** 8537
[30] Auld B A 1973 *Acoustic Fields and Waves in Solids* (New York: Wiley)
[31] Anon 1993 *Final Technical Report* Brite-Euram; BREU-0140
[32] Rehwald W 1973 *Adv. Phys.* **22** 721